Available on CMS information server

CMS NOTE -2020/004

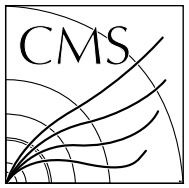

The Compact Muon Solenoid Experiment

CMS Note

Mailing address: CMS CERN, CH-1211 GENEVA 23, Switzerland

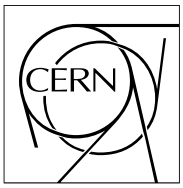

13 February 2020 (v6, 03 July 2020)

A semi-empirical model for preheater design to trigger CO_2 boiling for detector cooling

G. Baldinelli[a,b*], T. French[c], F. Bianchi[a,d], J. Daguin[c], A. Onnela[c], P. Tropea[c]

[a] INFN Sezione di Perugia - Italy,

[b] University of Perugia - Department of Engineering - Italy,

[c] CERN, Geneva, Switzerland,

[d] University of Perugia - Department of Physics and Geology.

[*] corresponding author

Abstract

The fluid properties of CO_2 make it an ideal medium for the cooling of tracking detectors in experiments at particle accelerators. Detectors such as the Compact Muon Solenoid Outer Tracker at CERN will be cooled to a nominal temperature of -35°C with CO_2 cooling to ensure the longevity of the silicon sensors. In theory, two-phase CO_2 cooling results in a very low temperature change along the detector tube, dependent only on pressure drop. Experimentally, however, superheating - the existence of a fluid in the liquid form above its boiling temperature - has been observed to occur frequently. This results in higher fluid temperatures and a poor heat transfer coefficient over the first section of the detector tube, disrupting the cooling performance of the detector and possibly leading to deterioration of the silicon sensors. In order to prevent superheating, a preheater is proposed to trigger nucleate boiling in the Compact Muon Solenoid Outer Tracker detector cooling tube just upstream of the sensors. A theoretical - semi-empirical - model for the preheater design is presented, starting from experimental data points. With this model, the triggering of nucleation can be characterised for tubes made of the same material as that tested and with the same surface cavity size. The model validation is promising, closely matching the trends from experimental results, and giving preheater specific powers significantly lower than those derived from spinodal theory.

A semi-empirical model for preheater design to trigger CO_2 boiling for detector cooling

G. Baldinelli[a,b*], T. French[c], F. Bianchi[a,d], J. Daguin[c], A. Onnela[c], P. Tropea[c]

[a] INFN Sezione di Perugia - Italy,

[b] University of Perugia - Department of Engineering - Italy,

[c] CERN, Geneva, Switzerland,

[d] University of Perugia - Department of Physics and Geology.

*corresponding author

Abstract

The fluid properties of CO_2 make it an ideal medium for the cooling of tracking detectors in experiments at particle accelerators. Detectors such as the Compact Muon Solenoid Outer Tracker at CERN will be cooled to a nominal temperature of −35°C with CO_2 cooling to ensure the longevity of the silicon sensors. In theory, two-phase CO_2 cooling results in a very low temperature change along the detector tube, dependent only on pressure drop. Experimentally, however, superheating – the existence of a fluid in the liquid form above its boiling temperature – has been observed to occur frequently. This results in higher fluid temperatures and a poor heat transfer coefficient over the first section of the detector tube, disrupting the cooling performance of the detector and possibly leading to deterioration of the silicon sensors. In order to prevent superheating, a preheater is proposed to trigger nucleate boiling in the Compact Muon Solenoid Outer Tracker detector cooling tube just upstream of the sensors. A theoretical – semi-empirical – model for the preheater design is presented, starting from experimental data points. With this model, the triggering of nucleation can be characterised for tubes made of the same material as that tested and with the same surface cavity size. The model validation is promising, closely matching the trends from experimental results, and giving preheater specific powers significantly lower than those derived from spinodal theory.

Keywords

Nucleate boiling; CO_2 electronics cooling; superheating; preheaters, R744.

Nomenclature

C	specific heat	[J/kg K]
D	tube diameter	[m]
f	friction coefficient	[-]
H	enthalpy	[J/kg]
h	convection coefficient	[W/m^2 K]
k	thermal conductivity	[W/m K]
L	preheater length	[m]
M	fluid mass flow rate	[kg/s]
Nu	Nusselt number	[-]
P	perimeter	[m]
p	pressure	[Pa, bar]
Pr	Prandtl number	[-]
Q	global heat flux	[W]
q	specific heat flux	[W/m^2]
r	radius	[m]
v	specific volume	[m^3/kg]
T	temperature	[K, °C]
y	distance from the inner tube surface	[m]
z	coordinate along the tube section	[m]

Subscripts

B	bulk
b	bubble
c	cavity
eq	equilibrium
i	inlet
l	liquid
lv	vaporisation
max	maximum
min	minimum
p	constant pressure
pr	preheater
sat	saturation
sub	subcooling
tip	higher part of the bubble
w	wall

Greek symbols

Δ	difference	[-]
ε	relative roughness	[-]
Θ_r	receding contact angle	[°]
ρ	density	[kg/m^3]
σ	surface tension	[N/m]

1. Introduction

The Large Hadron Collider (LHC) [1] is the world's largest and most powerful particle accelerator. Thanks to the performance of the LHC and its experiments, many highly relevant physics results have been obtained, including the discovery of the Higgs boson by the ATLAS (A Toroidal LHC ApparatuS) and CMS (Compact Muon Solenoid) experiments in 2012 [2] [3]. The LHC Long Shutdown 3 (LS3), scheduled to last from 2025 to mid 2027, will prepare the field for the High Luminosity phase of the LHC (HL-LHC). The HL-LHC upgrade will greatly expand the physics potential of the LHC, in particular for rare and statistically limited standard model and beyond standard model processes [4] [5]. The HL-LHC upgrade is accompanied by an upgrade programme of the CMS experiment, to maintain the performance of the detector and to fully profit from the HL-LHC capabilities, in spite of the challenging radiation levels and operating conditions. The CMS detector [6] needs to be substantially upgraded during LS3 in order to exploit the increase in luminosity provided by the HL-LHC [5]. The innermost part of CMS is the silicon tracking system, consisting of an Inner Tracker (IT) based on silicon pixel modules and an Outer Tracker (OT) made from silicon modules with strip and macro-pixel sensors. The tracker fulfils the task, among others, of providing tracking information for the momentum reconstruction of particles [4]. The total power to be removed from the tracking volume, due to electronics power dissipated locally and heat leaks from the surroundings, is expected to be about 100 kW for the Outer Tracker and about 50 kW for the Inner Tracker [8], including losses on cables inside the tracking volume. The cooling system must remove this heat load and maintain the silicon sensors at a temperature of −20°C or lower to limit the thermal effects of radiation damage. In order to achieve this cooling performance, evaporating CO_2 was chosen as refrigerant fluid [8]. The system will be designed for a nominal boiling point of the CO_2 at the detector outlet of −35°C, resulting in a coolant temperature of about −33°C at the location of the first silicon module, which is the warmest location along a cooling loop [8]. The properties of CO_2 make it an ideal medium for cooling of tracking detectors, in particular because of the ability to use smaller diameter, lower mass tubing than is required with conventional refrigerants or liquid cooling applications [7]. As the viscosity of CO_2 is low, it allows the use of small diameter tubes with higher flow speeds, which increases the heat transfer coefficient from the tube wall to the fluid. CO_2 is radiation hard, cheap, and environmentally friendly [9] [10] [11].

The CO_2 cooling plants provide a flow of CO_2 in liquid phase. The flow is distributed to 46 Outer Tracker and 24 Inner Tracker cooling segments through manifolds located in the experimental cavern [8]. Each of the cooling segments is then further split into parallel detector cooling loops at the entry to the tracker volume.

All detector cooling tubes are preceded by capillaries, which create the necessary pressure drop to reach the fluid saturation (boiling) point and ensure flow balancing across different loops on the same cooling segment. The temperature variation of the CO_2 in the silicon module region is nominally very small once the saturation curve is reached and evaporation has started, and only depends on the pressure drop along the detector tube. To ensure onset of evaporation, small preheaters (Fig. 1) with adjustable power corresponding to one to two detector modules (up to 10-20 W) will be installed upstream of the first modules in each cooling loop [8].

Experience has shown that superheating can occur [12], i.e. the fluid remains in the liquid state despite being above the boiling temperature at a given pressure [13]. This circumstance should be avoided in the detector for two main reasons [14] [15] [16]:

1. if superheating occurs in the cooling tubes serving the sensors, the resulting heat exchange is extremely poor; this is due to both the lower single-phase heat exchange coefficient – as there is no boiling – and the higher temperature of the CO_2;
2. the potential for a sudden phase transition with instantaneous release of the excess energy stored in the superheated liquid, e.g. due to a local pressure drop, creating a stress wave that could bring about mechanical damage not only in the thin-walled tubes but also in the surrounding sensors, cables, etc.

Researchers studying superheating generally agree on the danger deriving from this phenomenon, while different views are registered for the ways to prevent superheating:

- A liquid cannot be superheated up to the critical temperature: there is a limit to the maximum attainable temperature for any given liquid without boiling called the Superheat Limit Temperature. If this limit is reached before the fluid enters the zone to be cooled – achieving homogeneous volume boiling – the system is safe, even if this solution is very conservative and power consuming.
- Nucleate boiling can be triggered before the fluid enters the zone to be cooled. Two main approaches can be adopted for this purpose: a localized injection of heat or a sudden change in geometry. The first approach is achieved through low power, high heat flux devices, called “preheaters”; the second relies on the fluid inside the capillary already being superheated, and the tube diameter increasing at the exit of the capillary. In the latter case, there is one major concern: superheating in the capillary introduces the risk of boiling in the capillary. This could occur either naturally or due to particles from LHC collisions creating an effect similar to that observed in bubble chambers – a circumstance that would increase the flow resistance and affect flow balancing on a cooling segment with multiple evaporator loops.

As it is perceived to carry the lowest risk and a low overall power consumption, the use of high heat flux preheaters is considered the optimum solution for the CMS tracker upgrade cooling.

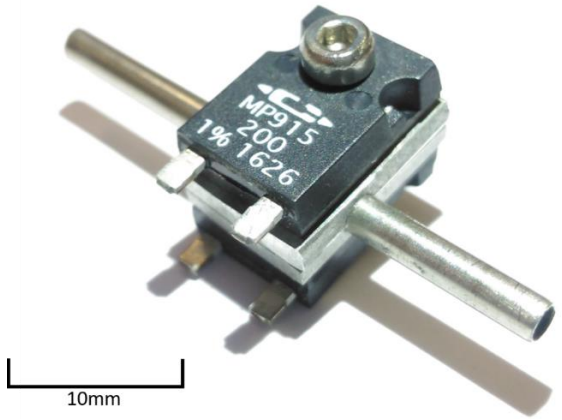

Figure 1 – An (unwired) electric preheater mounted on a cooling tube.

With the aim of describing the superheating phenomenon, Fig. 2 illustrates what happens theoretically (red line) when a compressed liquid (A) undergoes a depressurisation, evolving at a constant temperature up to B without changing its state from liquid. When point B is reached, the liquid is no longer stable and, in ordinary conditions without superheating, turns immediately to a two-phase configuration (a point on the BDF straight line) in which the liquid and vapour phases coexist at constant temperature and pressure up to F. At F, all the fluid is vapour and the isothermal curve continues with a depressurisation (G).

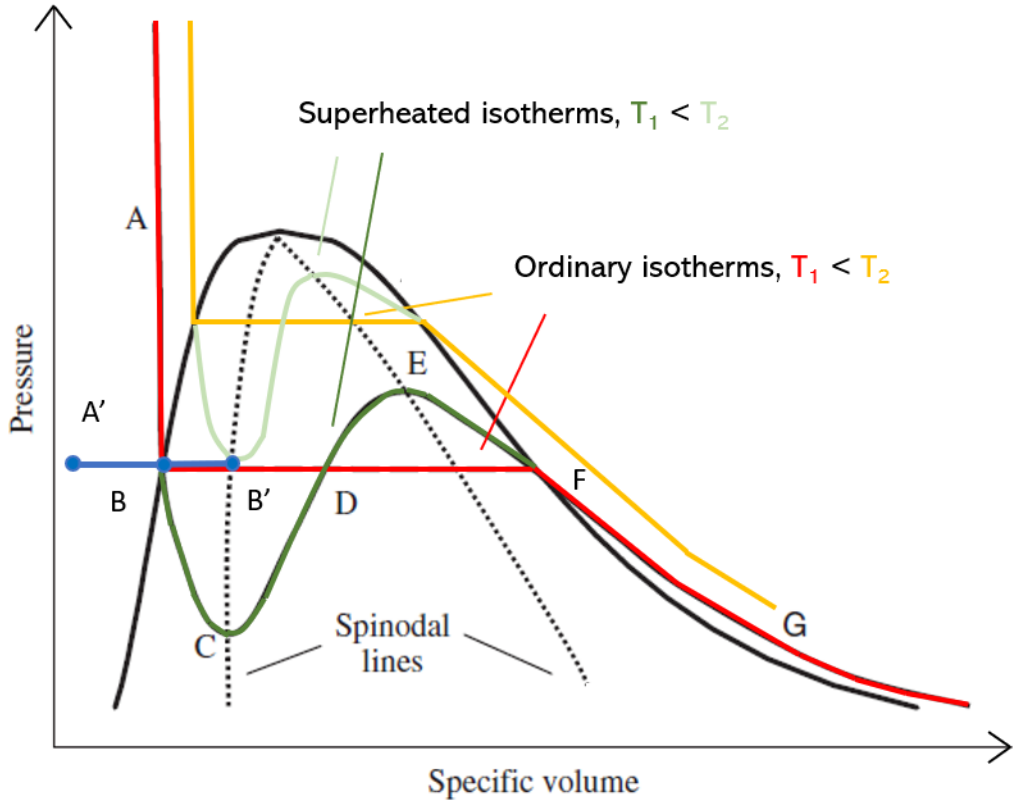

Figure 2 - p-v diagram of a generic fluid in the liquid-vapour zone.

When superheating occurs, the liquid phase can be present up to point C for pressures lower than the saturation pressure (left dark green line). On the other side of the two-phase region, the vapour phase can exist up to point E for pressures higher than the saturation pressure (right dark green line). The local minimum pressure (C) in an isotherm gives the point of maximum superheating. The locus of all such points is called the spinodal curve (Fig. 3).

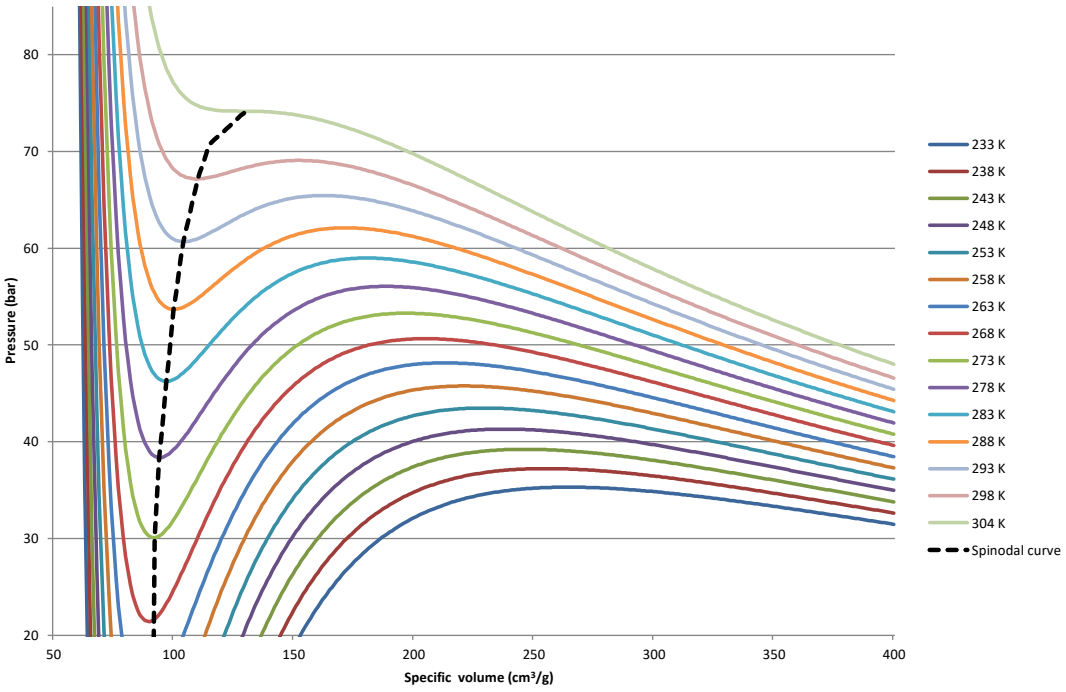

Figure 3 – Construction of the CO_2 spinodal curve from the isotherms using the Van der Waals equation of state.

The equilibrium and stability criteria described in eq. (1) force the isothermal process to comply with the bound:

$$(\partial p/\partial v)_T = 0 \tag{1}$$

The focal interest of this study is the module electronics and sensor cooling with approximately constant pressure transformations (blue line in Fig. 2). Moving from A' (subcooled liquid) to B and then from B to B' (superheating), the isotherm touching B' (light green line) represents the highest temperature that can be reached by the liquid phase for a given pressure: the Superheat Limit Temperature.
It is worth noting that different theoretical models for the equation of state [17] give significantly different spinodal curves and consequent different Superheat Limit Temperatures (Fig. 4).

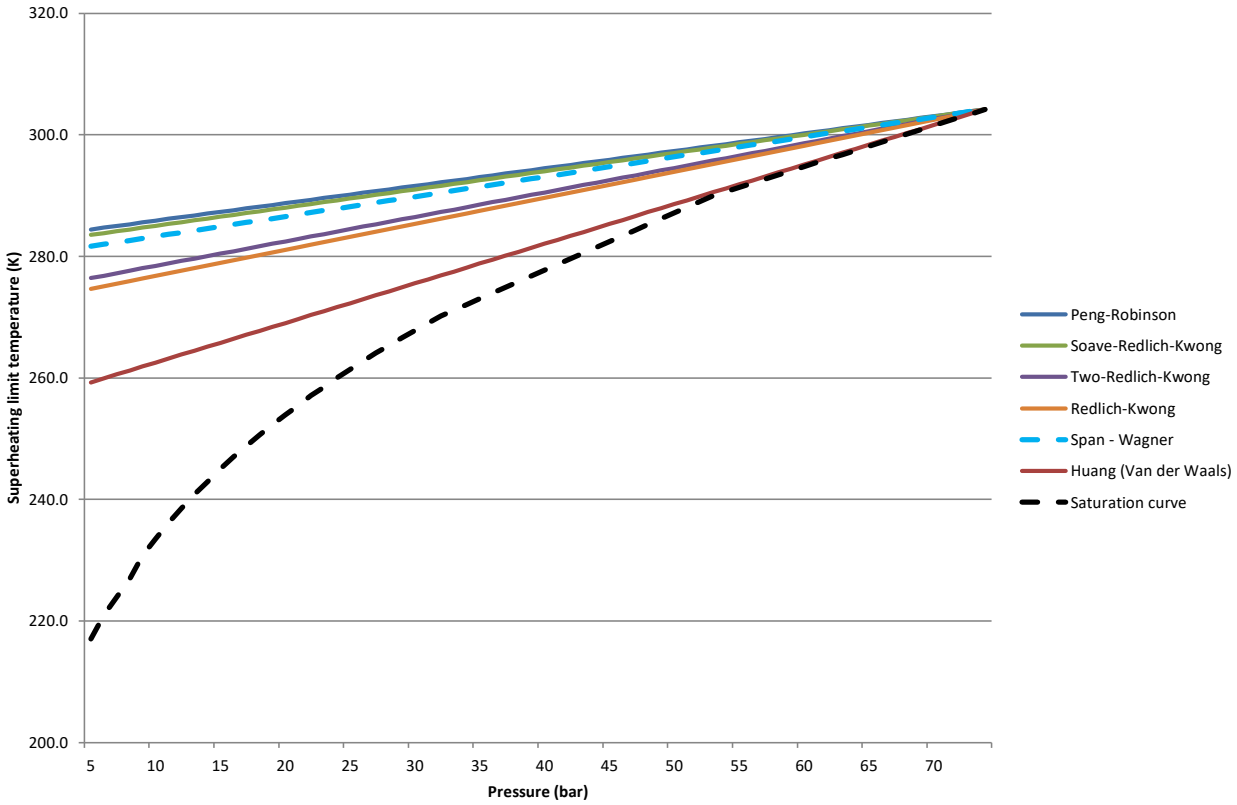

Figure 4 – Superheat Limit Temperatures of CO_2 using different theoretical models for the equations of state.

The Superheating Limit Temperature corresponds to the state of sole homogeneous boiling (the formation of vapour bubbles distributed in the entire volume of the superheated liquid mass), hypothesizing that no nucleate boiling (heterogeneous nucleation, with bubbles rising from singular points on solid walls) is present. Therefore, the limit value found – whichever is the model chosen for the equation of state – probably overestimates the power needed to initiate boiling. Nevertheless, if chosen as a design value for the preheater, it would represent a way to put the sensors "in a safe place" for each flow condition. On the other hand, the power required to reach the Superheating Limit Temperature is very high; if this was the power level needed in the Outer or Inner Tracker preheaters, it would be necessary to think of an independent powering system for the preheaters themselves, and also to enhance the cooling capacity of the CO_2 plants due to the increase in power. In such a scheme, each preheater may no longer be considered as producing roughly the same heat load as one module. This brings the problem to a very different level of complexity, requiring the development of dedicated powering hardware, and dedicated developments in the Detector Control System (DCS) and interlock system. Furthermore, the approach of designing the preheater to exceed the Superheating Limit Temperature value could be criticised for another reason: a large amount of power has to be absorbed by the liquid CO_2 in the preheater itself, perhaps many times more than that needed for initiating boiling, with the consequence that a considerable amount of liquid CO_2 evaporates in the preheater. It thus reduces the cooling capacity of the fluid which continues along the tube with the aim of extracting heat from the sensors and electronics. It can also result in approaching full vaporisation at the detector exit

instead of maintaining a vapour quality of about 33%, the limit chosen [8] to avoid safely the possible consequences of dryout being reached under specific working conditions. It is therefore necessary to design the preheater correctly, trying to prevent superheating and, at the same time, avoiding excessive preheater power consumption.
Superheating cannot occur at the silicon sensors if the power required to exceed the Superheating Limit Temperature value is supplied in a preheater, but it can also be avoided with lower preheater power, if nucleate boiling is activated.
An experimental way to design the preheater consists of constructing a test bench with tube circuits similar or equal to those planned to be installed in the tracker and carry out testing, assessing the minimum electric power needed for the preheater while changing influential parameters: tube diameter, tube material, tube length, mass flow rate, CO_2 pressure, subcooling level, and preheater length. We argue that the experimental approach is reliable and cannot be bypassed before the final implementation, being at the same time particularly onerous. At the aim of reducing or focusing the test bench efforts, a semi-empirical approach is illustrated in the next sections; the model, calibrated and validated with experimental tests, can assist to understand the dependence of the required preheater power on the parameters involved in the phenomenon.

2. Description of the model

The question of superheating is broken down into exploring the conditions for the Onset of Nucleate Boiling (ONB) occurring inside the preheater.
The necessary condition for the boiling incipience postulated by Hsu [18] has been used as the basis for many successive equations developed for ONB [19]. The bubble rises from the interior of a cavity present on a heated surface because of its roughness or local imperfections and establishes a shape dictated by the receding contact angle Θ_r on the walls of the cavity shown by interface 1 (Fig. 5). As the bubble grows, it is pushed up to the cavity mouth (interface 2). As the bubble keeps growing, it takes shapes 2, 3 and 4 until the contact angle reaches the critical value Θ_r on the heater surface.
Different nucleation criteria exist [20]; each of them states that, once a bubble has passed the condition of minimum radius, it will continue to grow. Hsu assumed that the limiting case corresponds to interface 4 with a fixed contact angle of 53.1°. Davies and Anderson [21] considered the contact angle establishment as the limiting stage, as depicted by interface 4. Sato and Matsumura [22] and Bergles and Rohsenow [23] considered a hemispherical bubble (interface 3) as the limiting case; here, the radius of curvature is the smallest during the bubble evolution and the contact angle is 90°.

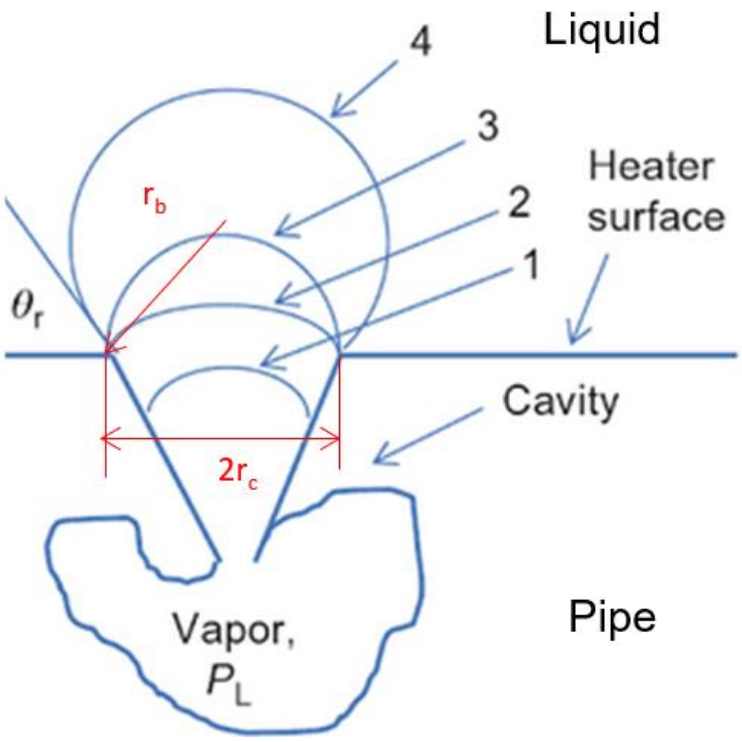

Figure 5 – Different stages of bubble growth.

The entire liquid-vapour interface of a bubble should be at a temperature above the minimum liquid superheat requirement for the bubble to guarantee nucleation. Since the temperature in the liquid reduces farther away from the heated tube surface, the lowest temperature in the liquid occurs at the tip of the growing bubble. A simple condition is then derived when the liquid temperature at the tip exceeds the minimum required temperature to feed the vapour bubble.
At a given cross section $\bar{z}$ of the heated cylindrical surface with a constant specific heat flux q_w (Fig. 6), the temperature T (red line) in the liquid at a distance y from the tube wall is obtained from the hypothesis of a linear temperature profile. This assumption appears quite realistic, specifically in the laminar sublayer near the tube wall, and it is made explicit in eq. (2) and (3):

$$\frac{k_l}{y}[T_w(\bar{z}) - T_l(y)] = h\left[T_w(\bar{z}) - T_{l,B}(\bar{z})\right] \tag{2}$$

$$T_l(y) = T_w(\bar{z}) - y\frac{h}{k_l}\left(T_w(\bar{z}) - T_{l,B}(\bar{z})\right) \tag{3}$$

where k is the thermal conductivity, h is the convection coefficient, l stands for liquid, w for wall and B for bulk.

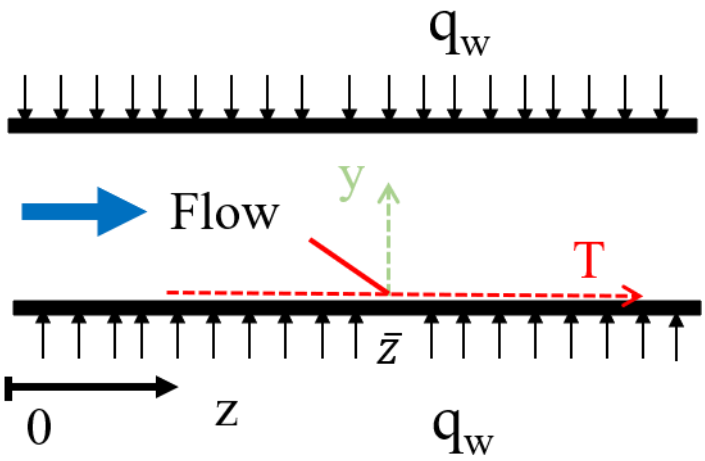

Figure 6 - Section of the tube with the coordinate reference system and liquid temperature trend near the wall.

The equilibrium theory provides the superheat equation (4) for the bubble nucleus [24]:

$$T_{l,eq} = T_{sat}(p_l) + \frac{2\sigma}{r_b}\frac{T_{sat}(p_l)}{\rho_v H_{lv}} \tag{4}$$

where p is the fluid pressure, σ is its surface tension, H_{lv} is the enthalpy of vaporisation, ρ the density, r the bubble radius, v stands for vapour, sat for saturation and b for bubble.
The bubble radius is linked to the cavity radius r_c by the simple relation (5):

$$r_b = r_c/sin\theta_r \tag{5}$$

With Sato and Matsumura [22] and Bergles and Rohsenow's [23] hypothesis, the hemispherical bubble is the limiting case, i.e. the receding contact angle $\Theta_r = 90°$, and then: $r_c = r_b = y_{b,tip}$.
The equilibrium condition is thus derived in eq. (6) when the liquid temperature at the bubble tip is equal to the value required to sustain the vapour bubble:

$$T_l(b, tip) = T_{l,eq} \tag{6}$$

Combining the previous equations with equations (3) and (4) yields the condition shown in quadratic equations (7) and (8) for nucleating cavities of specific radii:

$$r_c\frac{h}{k_l}\left[T_w(\bar{z}) - T_{l,B}(\bar{z})\right] - [T_w(\bar{z}) - T_{sat}(p_l)] + \frac{2\sigma}{r_c}\frac{T_{sat}(p_l)}{\rho_v H_{lv}} = 0 \tag{7}$$

$$r_c^2\frac{h}{k_l}\left[T_w(\bar{z}) - T_{l,B}(\bar{z})\right] - r_c[T_w(\bar{z}) - T_{sat}(p_l)] + 2\sigma\frac{T_{sat}(p_l)}{\rho_v H_{lv}} = 0 \tag{8}$$

the solution of which gives the two values $r_{c,min}$ and $r_{c,max}$, with the physical meaning shown in Fig. 7 [25].

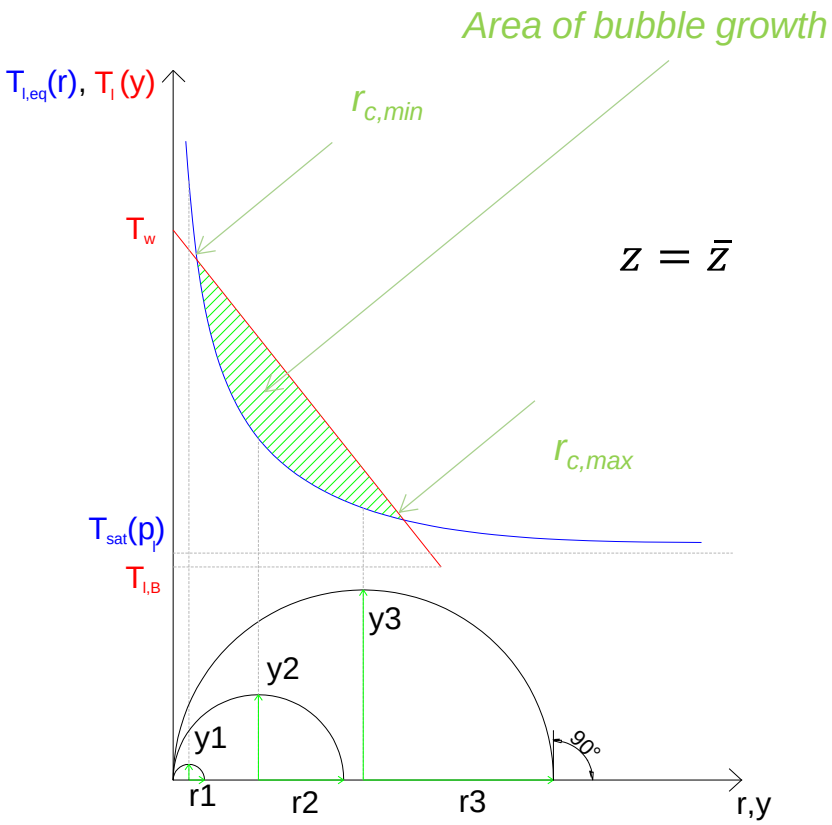

Figure 7 – Graphical representation of the bubble formation equations (in red the liquid temperature and in blue the bubble equilibrium temperature).

Defining the liquid subcooling and wall superheat in eq. (9) and (10):

$$\Delta T_{sub}(\bar{z}) = T_{sat}(p_l) - T_{l,B}(\bar{z}) \tag{9}$$

$$\Delta T_{sat}(\bar{z}) = T_w(\bar{z}) - T_{sat}(p_l) \tag{10}$$

and finally expressing with eq. (11) the heat per surface area transferred to the tube walls:

the combination of the previous equations gives the quadratic solutions for r_c, fixing the heat per surface area of the tube and the tube wall superheating.
The fluid properties are evaluated at the wall temperature in eq. (12), as their formation is quite close to the

$$q_w = h\left[T_w(\bar{z}) - T_{l,B}(\bar{z})\right] = h[\Delta T_{sat}(\bar{z}) + \Delta T_{sub}(\bar{z})] \tag{11}$$

$$r_{c,min}; r_{c,max} = \frac{k_l \, sin(\theta_r)\Delta T_{sat}(\bar{z})}{2q_w[1+cos(\theta_r)]} \times \left\{1 \mp \sqrt{1 - \frac{8\sigma T_{sat}(p_l) q_w [1+cos(\theta_r)]}{\rho_v H_{lv} k_l \Delta T_{sat}^2(\bar{z})}}\right\} \tag{12}$$

wall itself:

The minimum and maximum radii $r_{c,min}$ and $r_{c,max}$ of the active cavities are obtained from the negative and positive signs of the radical.
Many variations have been proposed to this model. A correction term on the previous equations has been proposed to take into account the bubble suppression effect of the thermocapillary force in microchannels [26]. Other researchers used a turbulent film temperature profile in the boundary layer instead of a linear trend [27], or implemented numerical simulations to assess the effect of the bubble on the thermal field [28].

Nevertheless, the semi-empirical nature of the original model discussed later justifies keeping the simpler approach described above.
If cavities with radius exactly equal to $r_{c,crit}$ of Fig. 8 are not present in the tube, a higher fluid temperature is needed, i.e. the radical term has to be larger than 0, shifting the fluid temperature curve upwards, to include cavities with radius ranging between $r_{c,min}$ and $r_{c,max}$. In this case, the necessary condition for boiling is the existence of cavities with radius $r_{c,min}$. This represents the limit for triggering boiling as when a bubble of this radius forms inside a cavity of the same radius, it can grow due to the fluid temperature being higher than the bubble temperature at increasing radii. The opposite cannot happen with $r_{c,max}$. The nucleate boiling issue is then solved if $r_{c,min}$ is found.

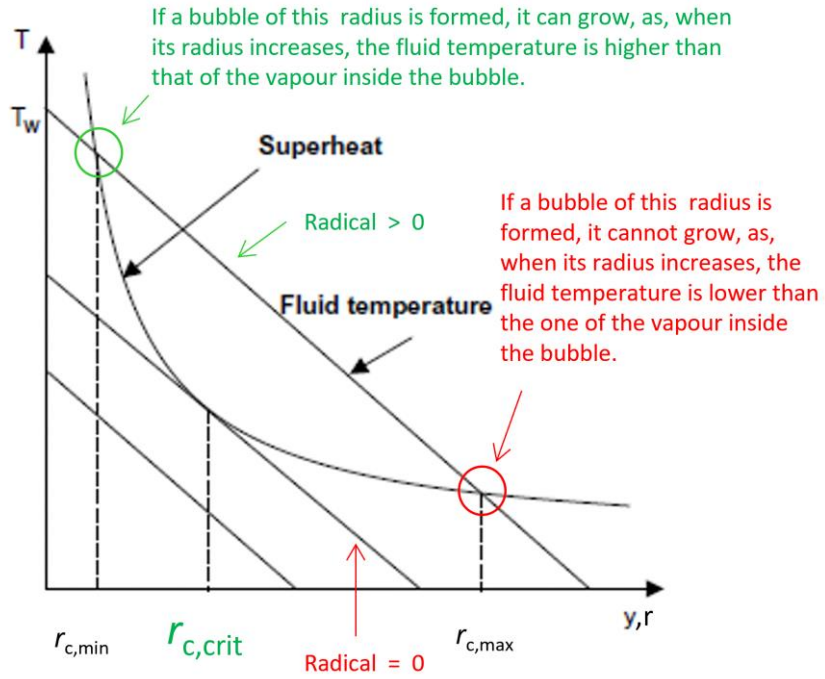

Figure 8 – Diagram for the definition of boiling triggering conditions.

The triggering of boiling can be reached both by increasing the cumulative applied heat, which means the fluid temperature line moves towards increasing z as the fluid heats up (Fig. 9a), and by increasing the specific heat flux, which steepens the gradient of the fluid temperature near the tube wall (Fig. 9b).

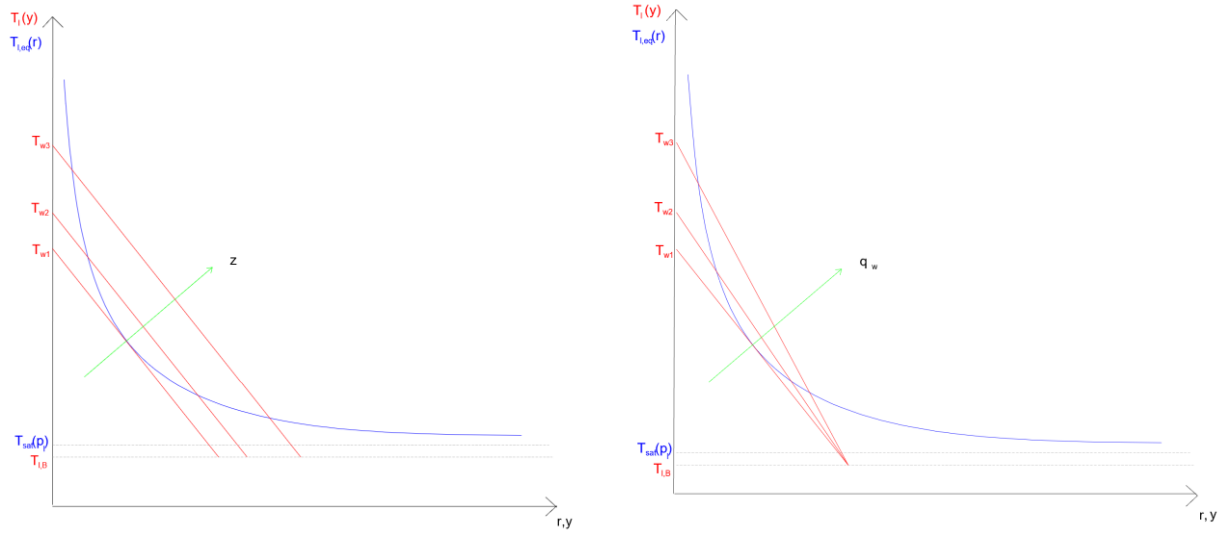

Figure 9a) - Wall temperature increase as the fluid travels along the tube with constant heat flux; 9b) - Wall temperature increase with increasing specific heat flux.

In equations (10) and (12), the only missing parameter is the wall superheating $T_w(\bar{z})$.
At a generic section $\bar{z}$, the local heat transfer between the tube and the liquid is given by the convection equation (11), where $T_{l,B}(\bar{z})$ is found in eq. (13) considering subcooled liquid entering a small hydraulic diameter channel at an inlet temperature $T_{l,B,i}$, assuming a uniform specific heat flux q_w, and steady-state conditions:

$$T_{l,B}(\bar{z}) = T_{l,B,i} + \frac{q_w P z}{M C_{p,l}} \tag{13}$$

where P is the section perimeter, $C_{p,l}$ is the liquid specific heat, M is the fluid mass flow rate, and $T_{l,B,i}$ is the inlet fluid temperature.
The total power given to the fluid by the preheater is given by the specific heat flux obtained from equation (12) in correspondence to the minimum radius $r_{c,min}$, multiplied by the contact area between the pipe and the preheater:

$$Q_{pr} = q_w P L = \frac{k_l \sin(\theta_r)}{[1+\cos(\theta_r)] r_{c,min}} \left[\Delta T_{sat}(\bar{z}) - \frac{2\sigma T_{sat}(p_l)\sin(\theta_r)}{\rho_v H_{lv} r_{c,min}} \right] P L \tag{14}$$

The convection coefficient h has to be derived. If the flow is turbulent, h can be obtained from the Nusselt number derived in eq. (15) by the Gnielinsky correlation [29]:

$$Nu = \frac{hD}{k_l} = \frac{(f/8)(Re-1000)Pr}{1+12.7\sqrt{f/8}\left(Pr^{2/3}-1\right)} \tag{15}$$

which remains accurate in the following ranges of Prandtl and Reynolds numbers: $0.6 < Pr < 10^5$ and $2{,}300 < Re < 10^6$.
Trying to take into account the entrance region effect, where the flux is mechanically fully developed but its thermal history begins in the preheater or in the sensors, the correction given by the Geankoplis equation (16) [30] is provided:

$$\frac{Nu_L}{Nu} = 1 + \left(\frac{D}{L}\right)^{0.7} \tag{16}$$

which is valid for turbulent flow, at $2 < L/D < 20$. L is the length of the preheater, f is the friction coefficient that can be retrieved by the Moody diagram or by the simplified Haaland equation (17), where ε is the relative roughness:

$$\frac{1}{\sqrt{f}} = -1.8 log\left[\left(\frac{\epsilon/D}{3.7}\right)^{1.11} + \frac{6.9}{Re} \right] \tag{17}$$

If the flow is laminar, $Nu = 4.36$ and $f = 64/Re$. An equation (18) covering all the regimes can be used to make the calculation simpler [31]:

$$f = 8 \sqrt[12]{\left(\frac{8}{\mathrm{Re}}\right)^{12} + \left\{ \left[-2.457 \ln\left(\left(\frac{7}{\mathrm{Re}}\right)^{0.9} + 0.27\epsilon \right) \right]^{16} + \left(\frac{37530}{\mathrm{Re}}\right)^{16} \right\}^{-1.5}} \tag{18}$$

It is generally difficult to assess the microscopic structure of tubes with the purpose of understanding if cavities of the right radius $r_{c,min}$ are present for the activation of nucleate boiling. The value of surface roughness could give an indication and it is often an available parameter. It is defined as the average absolute deviation of the roughness irregularities from the mean line over one sampling length. It represents an average value of the peaks and valleys with respect to the average profile, therefore it does not give precise information on the cavity radii. For instance, if a surface roughness increase produces only high diameter cavities, they will be filled with liquid and they will not act as nucleation centres [32]. As it is not possible to characterize the cavity sizes of the tube through a measurement of the surface roughness alone, experimental data with the real fluid are needed as inputs to this model.

3. Experimental setup

The test setup used to validate this model uses spare parts of the present CMS TOB (Tracker Outer Barrel): three support structures for the silicon sensors, cooled with the same size tubes as those proposed for the CMS Tracker Phase-2 Upgrade TB2S (Tracker Barrel for 2S modules, where 2S modules are silicon modules with two strip sensors) design (2.0 mm inner diameter and 2.2 mm outer diameter [8], with tube material of Cu70Ni30 as one of the possible alternatives), installed in an insulated box in a temperature-controlled cold room at CERN. Each TOB support structure has a cooling tube that is 2.5 metres long, and the three tubes are connected in series, as the TB2S tubes will also be connected in series in the new detector (Fig. 10).

The cooling tube in each TOB support structure has 24 cooling inserts glued to the tube. These cooling inserts are 40 mm long machined pieces of aluminium, which transmit the module heat to the tube. The modules are represented by 24 x 200 Ω resistors (Caddock MP915 with a resistance of 200Ω +/− 1%) per TOB support structure, electrically connected in parallel providing a nominal 2W per cooling insert. This simulates an average power consumption of the future modules installed in this part of the tracker. The voltage applied to the resistors is controlled by a calibrated power supply.

Figure 10 – The test setup in an insulated box.

The resistors are mounted onto 1.5 mm thick aluminium sheets of the same outer dimensions as the resistors using thermal grease (Dowsil 340 heat sink compound, k = 0.6 W/mK). A 1.4 mm brass screw is passed through the mounting hole in the resistor and the aluminium sheet and screwed into the existing threaded hole in the TOB support structure cooling insert, clamping the pieces together to ensure a good thermal contact (Fig. 11).

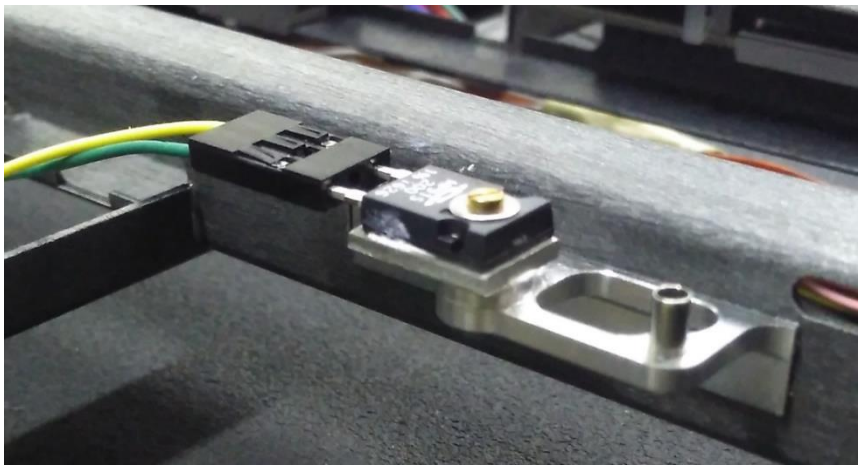

Figure 11 – Mounting of a dummy load resistor to a cooling insert.

A TRACI 2.3 plant [33] is used to provide liquid CO_2 to the experiment at a controlled temperature and mass flow rate. The TRACI is located outside of the cold room and is connected to the box inside the room via an insulated coaxial pipe. The experiment is connected to the coaxial pipe via separate, insulated 3.0 mm inner diameter / 5.0 mm outer diameter annealed copper tubes. A piping and instrumentation diagram is provided in Fig. 12.

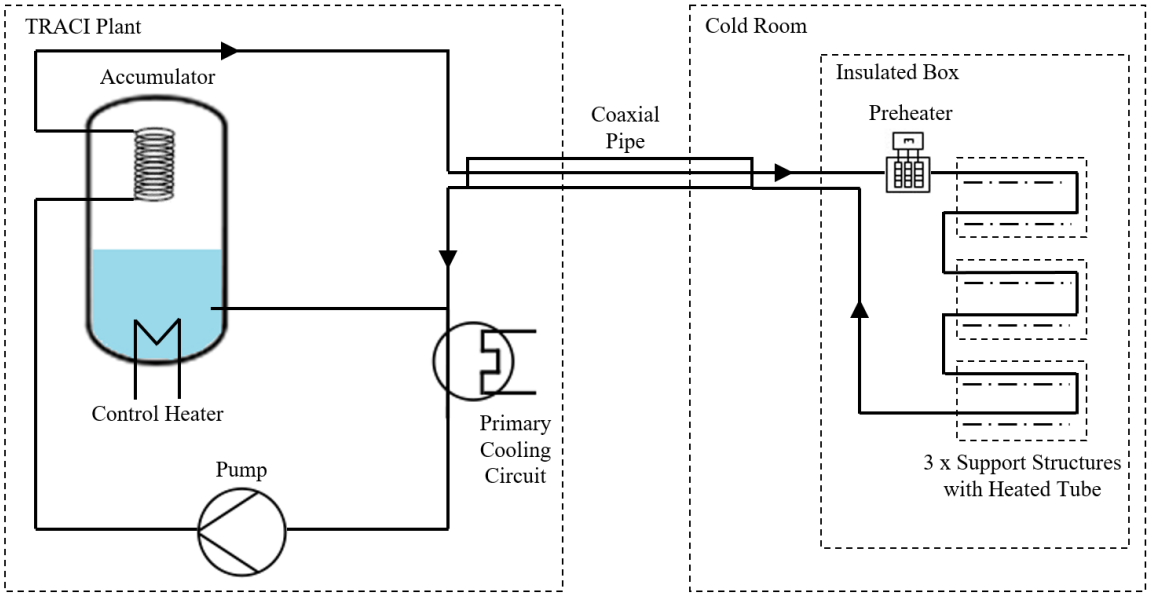

Figure 12 – Piping and instrumentation diagram of the test setup.

The temperature of the cold room can be lowered to the same temperature as the fluid when testing. This reduces the heat leak significantly, essentially creating a (close to) adiabatic test. By comparing the temperature increase of the liquid in the heated region to the theoretical increase based on the specific heat capacity, measurements show that on average, at nominal conditions, 93% of the electrical power from the power supply is transferred to the CO_2 through the heaters, with a variation of ±5%. The losses are principally due to convection and radiation from the heaters to the colder environment as well as electrical dissipation in the wires. The 7% reduction factor has been applied to the stated power of the dummy module heaters and preheaters. The minimum CO_2 temperature used as a set point in these tests is −25°C, with an average room temperature of approximately −24°C.

The temperature distribution is mapped using PT100 resistance temperature detectors (RTD, accuracy class: 1/3 DIN) glued in place using room-temperature-vulcanizing silicone (Electrolube TCOR75S, k = 1.8 W/mK) to the outside of the tube and cooling inserts. Blocks of insulating foam were glued around each RTD to minimise the effects of air temperature on the measurements. Sensors were glued onto 19 locations on the tubes, onto 8 cooling inserts, 8 resistor aluminium plates, and 2 preheater aluminium plates. Other sensors were used for the air temperature inside and outside the box. The temperatures are read via programmable transmitters (output 4-20 mA) connected via the analogue input modules of an NI cDAQ chassis to LabVIEW.

A preheater (one Caddock MP915, 10Ω +/− 1% with two grooved aluminium plates clamped around the tube by a screw) is mounted on a short, replaceable tube just before the first support structure inlet with thermal grease to improve the thermal contact (Fig. 1). The contact span between the grooved aluminium plates of the preheater and the tube comes in three different lengths: 16 mm, 8 mm and 1.5 mm. A second power supply is used to power the preheater resistor. The replaceable tube can be changed to modify the diameter, with different grooved aluminium plates used to accommodate the different pipe outer diameters.

The test box is flushed with 2.77 x10^{-4} m^3/s dry gas in standard conditions to avoid condensation although, with the temperature and humidity of the volume controlled by the room climatization unit, this is not strictly necessary.

The tests are carried out by letting the liquid CO_2 flow through the experiment at a given mass flow rate. The heating resistors are powered on all at the same time and are allowed to stabilise in temperature over

approximately 10 minutes. At this stage, CO_2 superheating has been seen to occur almost every time, with temperatures recorded of over 10°C higher than the saturated fluid temperature in some cases. The subcooling of the inlet fluid is indirectly controlled by the pressure drop in the experiment, as the coaxial pipe acts to set the inlet liquid to the same temperature as the outlet two-phase fluid. For a given tube geometry, the pressure drop varies as a function of the mass flow rate, set point temperature, and heater power, with a design range for the operating pressure of between 17 and 50 bar. After reaching steady-state conditions, and if the superheating effect is observed, all temperature values are recorded and plotted as a function of their position along the tube.

The first step of the model calibration is to calculate the radii of cavities in the given tube. The experimental values required are taken from the point at which nucleate boiling is triggered for a given saturation temperature T_{sat}. These values are: the cumulative applied power up to the trigger location, the surface area of the heated tube up to the trigger location (combined these give the heat flux q_w), and the fluid superheating $\Delta T_{sat}(\bar{z})$ in the tube at the trigger location. In Fig. 13, for instance, feeding the tube with a total power Q of 200 W through the heating resistors, the boiling is triggered by just the heating resistors – without preheater – between 50 W and 70 W (the granularity of the temperature sensor positions means there are no temperature sensors between 1,800 mm and 2,600 mm). The superheated liquid reaches a temperature not lower than −11°C from a saturation temperature of −23°C: the temperature reached could be slightly higher in the region where the instruments are missing.

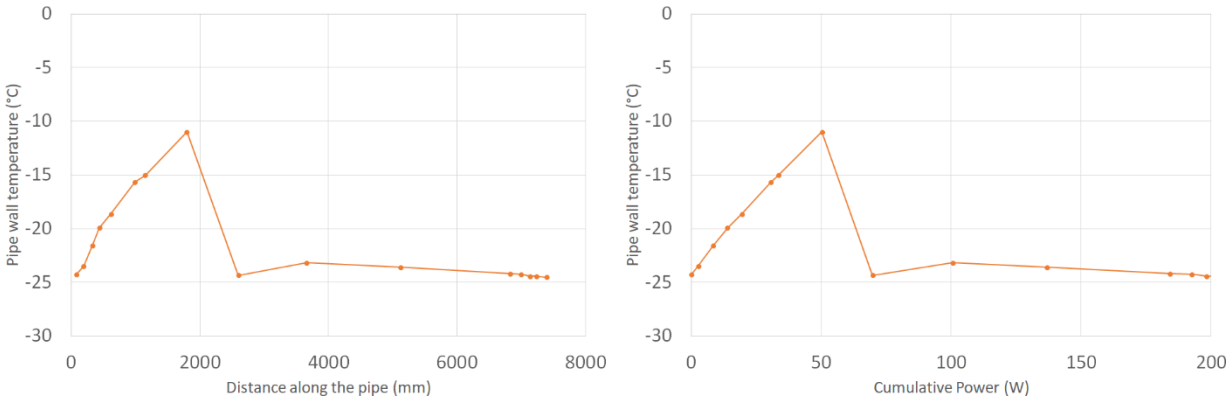

Figure 13 – Temperature along the tube vs. distance from the inlet and cumulative power supplied (T_{sat} = −23°C; M = 0.00148 kg/s; D = 0.002 m; Q = 200 W).

Inserting the values of the wall superheating measured by the temperature sensors and the specific heat flux at the triggering of boiling into the cavity radius equation (12), $r_{c,min}$ and $r_{c,max}$ are obtained; these values are a specific characteristic of the measured tube.

The parameters of the previous equations have to be calculated at the proper liquid temperature, therefore an iterative process is needed [34].

Once the tube has been characterised in this way, the performance of a preheater attached to this tube can be deduced from the model. If a parameter is to be varied (tube diameter, liquid mass flow rate, saturation temperature, heat flux, preheater length, subcooling level, etc.) the same equations have to be used, but $r_{c,min}$ is now a known term, while $T_w(\bar{z})$ can be found through equations (9), (10), (11) and (12). If the pipe material is to be varied, or the manufacturing process, this will very likely imply a different tube wall cavity size and the model validation must be repeated for the new tube.

The value of $T_w(\bar{z})$ within the preheater, retrieved from the previous equations, has to be compared with that obtained from heating along the tube up to a distance z. If the calculated value of $T_w(\bar{z})$ is higher than that obtained by the equations using $r_{c,min}$, nucleate boiling is active in section $\bar{z}$ and the preheater is predicted to dispel the superheating. The opposite occurs – no nucleate boiling – if $T_w(\bar{z})$ derived from the tube heating is lower than the value derived from $r_{c,min}$. The heat transferred from the preheater to the tube per contact surface unit q_w can be easily measured, as the preheater is a resistor; nevertheless, not all the heat goes to the CO_2 through the contact surface itself. The tubes are generally made of a conductive material, therefore, some of the heat flows laterally and has to be considered lost in the previous equation. A model, based on the two-dimensional heat transfer through a cylindrical tube, is included in the calculations to take this effect into account.

4. Model validation

The semi-empirical approach – a theoretical model calibrated with test results – previously described has been validated using the experimental setup described in the previous section.

Once the calibration has been carried out for a given tube geometry without a preheater, and the boundary conditions such as preheater length and heat flux per surface unit are defined, the other variables can be computed to understand the tube wall superheating temperature needed on the tube wall itself to start the nucleate boiling. This temperature has to be compared with the tube wall temperature obtained by the convection heat exchange at the end of the heated length: if the latter is higher than the former, nucleate boiling occurs, otherwise, nucleate boiling is prevented.

The preheater trigger power was measured experimentally by raising the preheater power gradually in 0.5 W or 1.0 W increments, until boiling was triggered at the preheater: the preheater temperature was observed to drop suddenly. After this, the temperature profile in the tube collapses to the expected two-phase distribution. Figure 14 shows the plots of the pipe wall temperature at different preheater feeding power; the preheater is located at 0 x-coordinate, the 24 heating resistors are equally distributed (every 30 cm) along the pipe, and the temperature sensors are positioned exactly on the curve marks. The tests were carried out up to three times for each data point and all the data points have been plotted in the following graphs.

In terms of experimental error, the systematic uncertainties shown in Table 1 have been calculated, starting from the manufacturers' specifications.

Table 1 – Estimation of systematic uncertainties for the measured parameters.

Variable	Uncertainty
Tube wall temperature	±0.1°C
Dummy power (at 2 W)	±5%
Preheater power (at 8 W)	±5%
Mass flow rate	±0.06 g/s

Uncertainty bars have been included in the preheater power plots, but omitted in the temperature profile plots (Figures 13 and 14) for clarity of presentation and due to the uniform ±0.1°C error. The triggering power was recorded as the range in which superheating disappeared, meaning that nucleation could have been triggered anywhere between the maximum and minimum values in the range. The error bars have been adjusted to include this uncertainty.

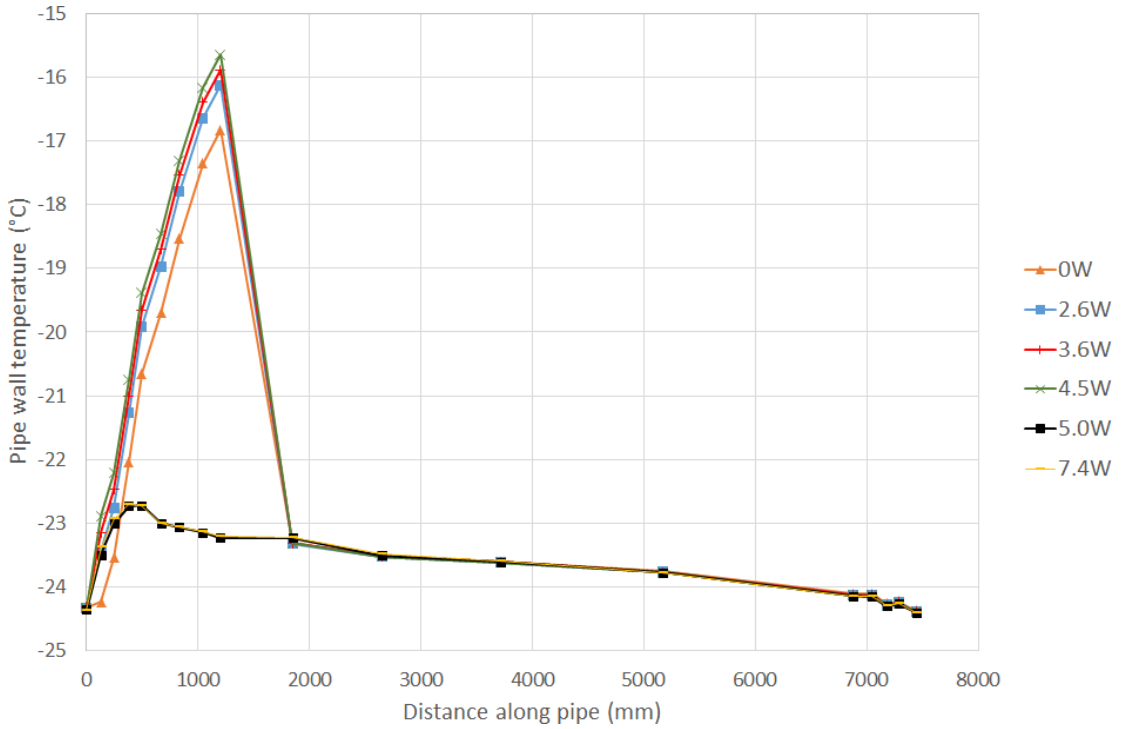

Figure 14 – Triggering the collapse of superheating through the step-wise increase of the preheater power (T_{sat} = −23°C; M = 0.00140 kg/s; D = 0.002 m; Q = 134 W).

The following figures show the results of the validation process, comparing the output of the semi-empirical model expressed in equation (14) to the preheater trigger power measured experimentally.
Figure 15 reports the preheater trigger power variation with the preheater length, Fig. 16 with the saturation temperature, Fig. 17 with the mass flow rate, Fig. 18 with the preheater tube internal diameter and Fig. 19 with the subcooling. The latter is a dependent variable and it is experimentally modified by changing the pressure drop along the pipe, which in turn can be changed by varying the saturation temperature and the mass flow rate.
The error bars include the uncertainty of the preheater power measurement and the discrete power steps for the boiling trigger: the data point is placed at the maximum of the range and the error bar extends lower, down to the minimum of the trigger interval.

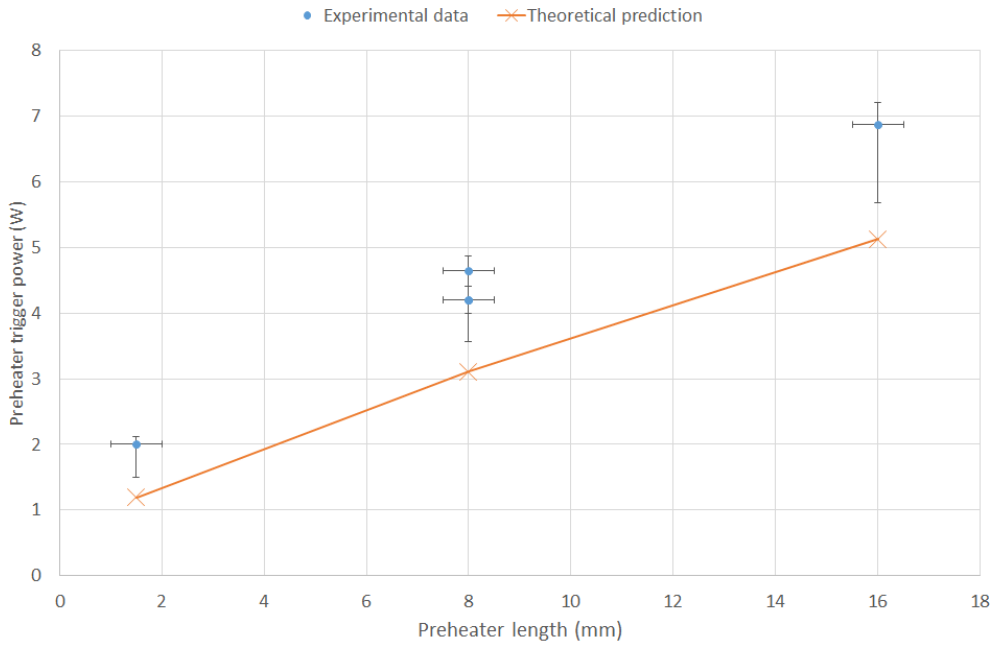

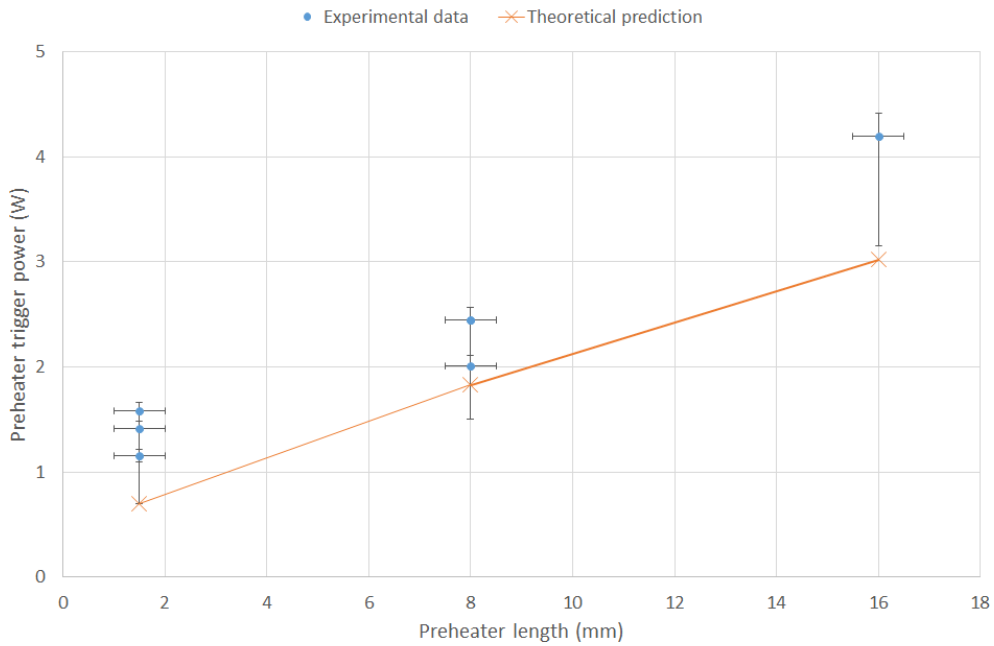

Figure 15 – Comparison of experimental data and semi-empirical model theoretical prediction of the minimum preheater power required to trigger boiling as a function of the preheater length: T_{sat} = −23°C (top) and T_{sat} = −7°C (bottom)
(M = 0.00140 kg/s; D = 0.002 m; Q = 134 W).

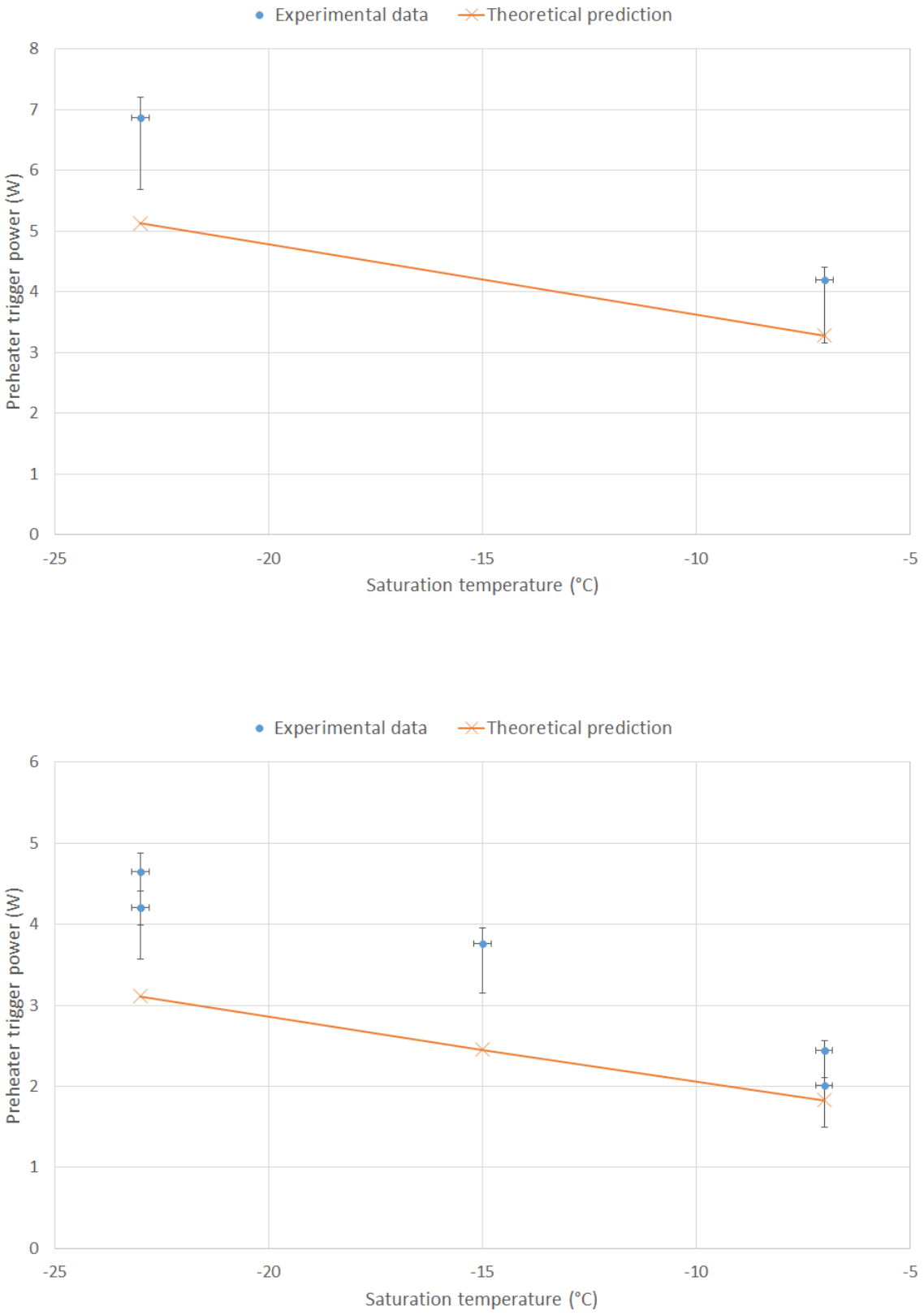

Figure 16 – Comparison of experimental data and semi-empirical model theoretical prediction of the minimum preheater power required to trigger boiling as a function of the saturation temperature: preheater length = 0.016 m (top) and 0.008 m (bottom)
(M = 0.00140 kg/s; D = 0.002 m; Q = 134 W).

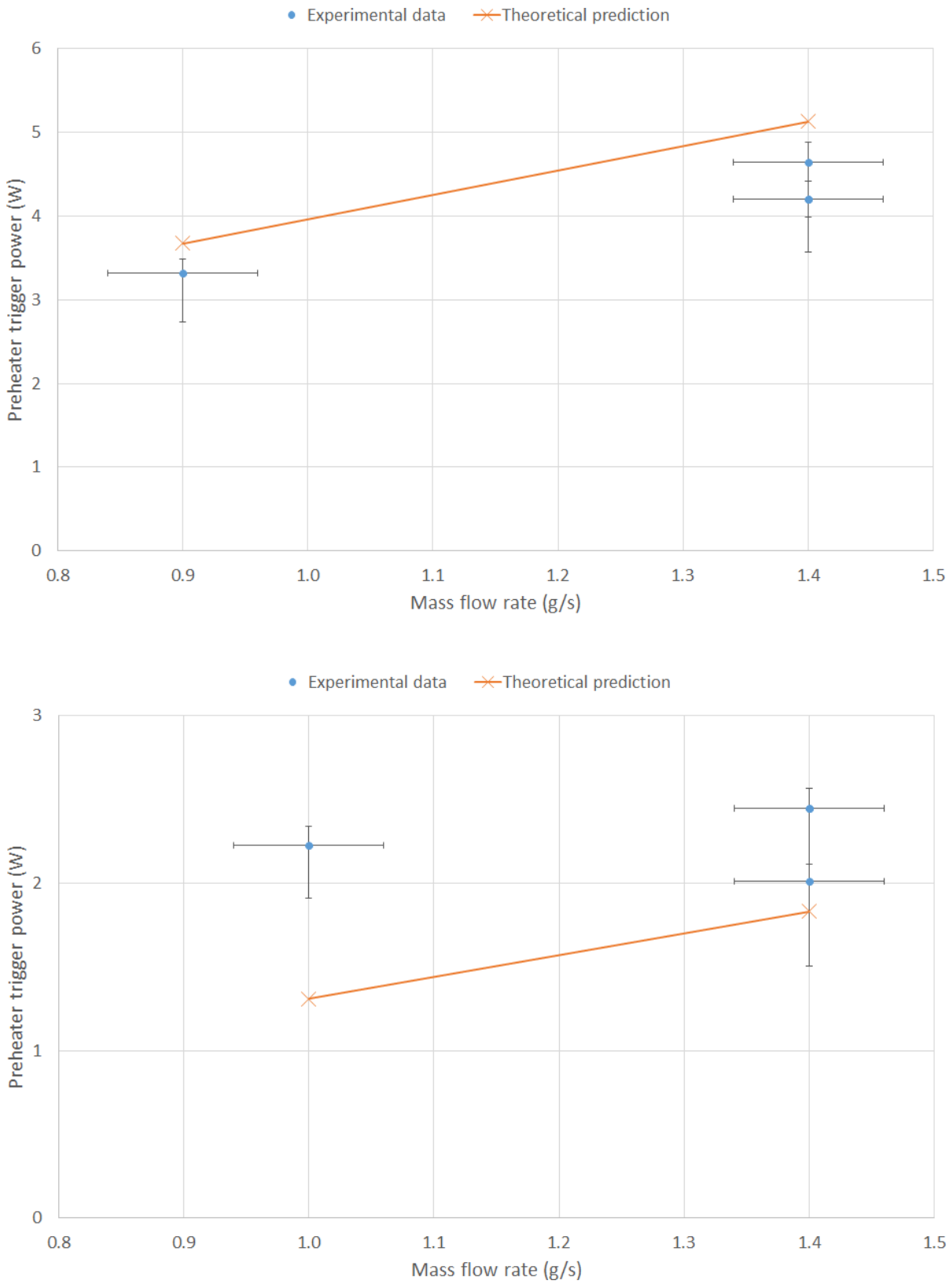

Figure 17 – Comparison of experimental data and semi-empirical model theoretical prediction of the minimum preheater power required to trigger boiling as a function of the fluid mass flow: T_{sat} = −23°C; L = 0.016 m (top) and T_{sat} = −7°C; 0.008 m (bottom) (D = 0.002 m; Q = 134 W).

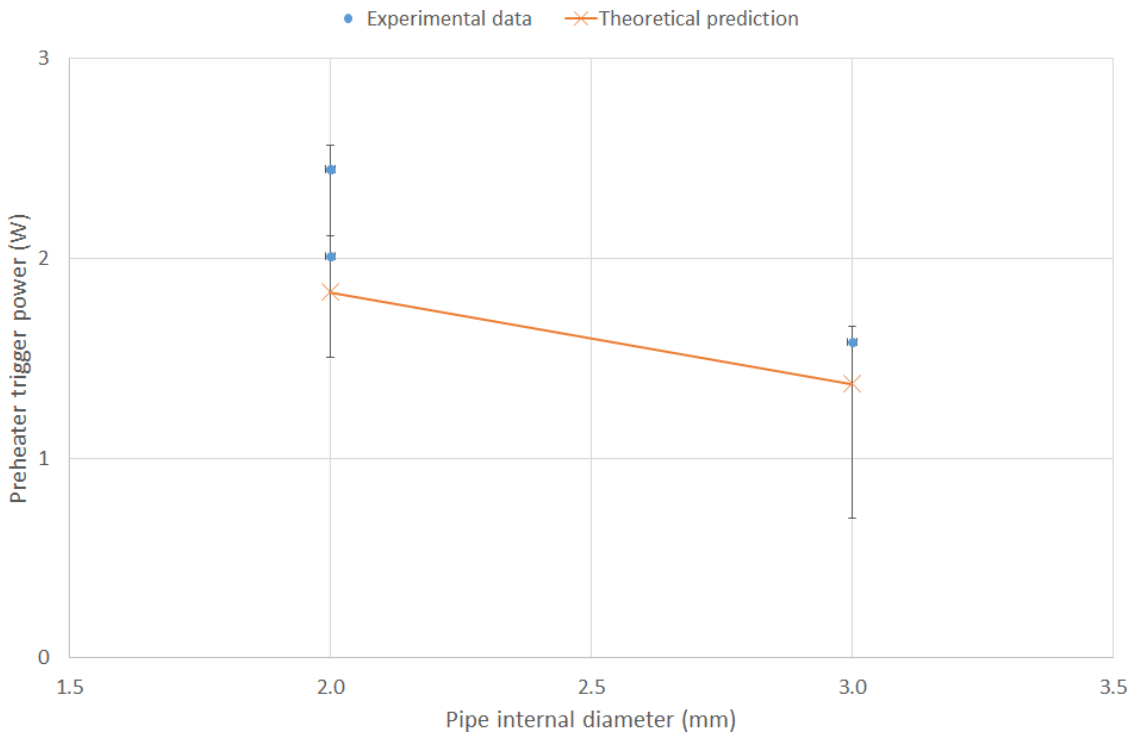

Figure 18 – Comparison of experimental data and semi-empirical model theoretical prediction of the minimum preheater power required to trigger boiling as a function of the preheater tube internal diameter
(L = 0.008 m; T_{sat} = −7°C; M = 0.0014 kg/s; Q = 134 W).

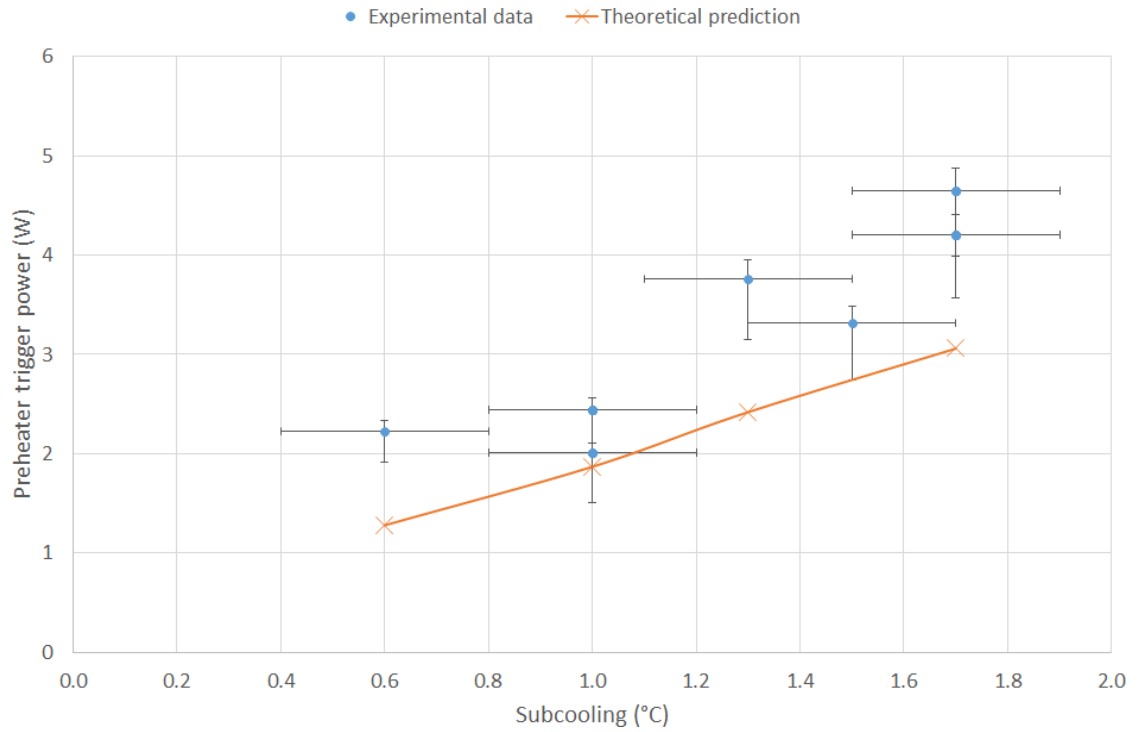

Figure 19 – Comparison of experimental data and semi-empirical model theoretical prediction of the minimum preheater power required to trigger boiling as a function of the subcooling
(L = 0.008 m; T_{sat} = −7 ÷ −23°C; M = 0.0010÷0.0014 kg/s; Q = 134 W).

5. Discussion

The semi-empirical model seems to slightly underestimate the power needed to trigger boiling, when compared to the experimental data. Nevertheless, the model itself seems to catch the expected trends of the minimum preheater specific power with respect to the parameters involved:

- the specific power required in the preheater increases with increasing preheater length;
- the specific power required in the preheater decreases with increasing saturation temperature;
- the specific power required in the preheater increases with increasing fluid mass flow. Some of the experimental data at $T_{sat} = -7$°C seem in contrast with the model trend; however, the error bars are wide enough to justify an upwards-sloping line;
- the specific power required in the preheater decreases with increasing tube internal diameter;
- the specific power required in the preheater increases with increasing subcooling. Also here, some of the experimental values at ΔT_{sub} = 1.0°C slightly diverge from the model, but again the error bars accommodate the model.

All these features may be derived by thermodynamic considerations, but the model gives additional quantitative information, once calibrated.

6. Conclusions

Superheating is observed frequently in tests of small diameter cooling tubes carrying liquid CO_2. In order to prevent superheating in the delicate sensor region of particle physics tracking detectors, a number of solutions are possible. Heating the fluid to reach the spinodal curve is guaranteed to work, however it leads to unnecessarily high additional power load on the cooling system. The solution presented here uses preheaters to trigger nucleate boiling in the detector cooling tube just upstream of the sensors. Preheater sizing can be determined from experiment alone, but the number of individual test measurements required to optimise the design might prove prohibitive. A semi-empirical model for the preheater design is proposed: starting from a few experimental data points, the triggering of nucleation can be characterised for tubes made of the same material as that tested and with the same surface cavity size. The model validation is promising, closely matching the trends from experimental results. A preheater can be designed for a specific application, using the proposed model for the characterised tube over a range of specified boundary conditions such as: tube diameter, liquid mass flow rate, saturation temperature, heat flux, preheater length, subcooling level, etc. The model is, in principle, applicable to any pure refrigerant fluid, however, there are many fields to be more deeply investigated, such as the effect of gravity, tube material and roughness.

References

[1] L. Evans and B. Bryant (editors), “LHC Machine”, 2008 JINST **3** S08001, doi:10.1088/1748-0221/3/08/S08001.

[2] ATLAS Collaboration, “Observation of a new particle in the search for the Standard Model Higgs boson with the ATLAS detector at the LHC”, Phys. Lett. **B 716** (2012) 1, doi:10.1016/j.physletb.2012.08.020, arXiv:1207.7214.

[3] CMS Collaboration, “Observation of a new boson at a mass of 125 GeV with the CMS experiment at the LHC”, Phys. Lett. B 716 (2012) 30, doi:10.1016/j.physletb.2012.08.021, arXiv:1207.7235.

[4] CMS Collaboration, “Technical Proposal for the Phase-II Upgrade of the CMS Detector”, CERN-LHCC-2015-010, LHCC-P-008, CMS-TDR-15-02 (2015), http://cds.cern.ch/record/2020886?ln=it.

[5] CMS Collaboration, “Updates on Projections of Physics Reach with the Upgraded CMS Detector for High Luminosity LHC”, CMS-DP-2016-064 (2016), https://cds.cern.ch/record/2221747.

[6] CMS Collaboration, “The CMS experiment at the CERN LHC”, 2008 JINST 3 S08004, doi:10.1088/1748-0221/3/08/S08004.

[7] B. Verlaat, ”Controlling a secondary 2-phase CO_2 loop using a 2-phase accumulator”, ICR07-B2-1565, International Conference of Refrigeration, Beijing, China (2007).

[8] CMS Collaboration “The Phase-2 Upgrade of the CMS Tracker - Technical Design Report”, CMS-TDR-014 (2017), https://cds.cern.ch/record/2272264?ln=it.

[9] A. Kneer, M. Wirtz, T. Laufer, B. Nestler, S. Barbe, “Experimental investigations on pressure loss and heat transfer of two-phase carbon dioxide flow in a horizontal circular pipe of 0.4 mm diameter”, International Journal of Heat and Mass Transfer 119 (2018) 828-840.

[10] J. Linlin, L. Jianhua, Z. Liang, L. Qi, X. Xiaojin, “Characteristics of heat transfer for CO_2 flow boiling at low temperature in mini-channel”, International Journal of Heat and Mass Transfer 108 (2017) 2120-2129.

[11] R. Mastrullo, A.W. Mauro, A. Rosato, G.P. Vanoli, “Carbon dioxide heat transfer coefficients and pressure drops during flow boiling: Assessment of predictive methods”, International Journal of Refrigeration 33 (2010) 1068-1085.
[12] K. Sliwa, P. Dziurdzia, D. Giakoumi, B. Verlaat, L. Zwalinski, N. Suzzi, “CO_2 superheating and boiling onset measurements in the ATLAS CO_2 cooling system”, Forum on Tracker Detector Mechanics, CPPM Marseille, France 3-5 July (2017).
[13] M. Das, B. K. Chatterjee, B. Roy, S. C. Roy, “How high can the temperature of a liquid be raised without boiling?”, Physical Review E 62, 5843 (2000).
[14] G. A. Pinhasi, A. Ullmann, A. Dayan, “1D plane numerical model for boiling liquid expanding vapor explosion (BLEVE)”, International Journal of Heat and Mass Transfer 50 (2007) 4780-4795.
[15] J.M. Salla, M. Demichela, J. Casal, “BLEVE: A new approach to the superheat limit temperature”, Journal of Loss Prevention in the Process Industries 19 (2006) 690-700.
[16] T. Abbasi, S.A. Abbasi, “Accidental risk of superheated liquids and a framework for predicting the superheat limit”, Journal of Loss Prevention in the Process Industries 20 (2007) 165-181.
[17] G.A. Pinhasi, A. Ullmann, A. Dayan, “Modeling of flashing two-phase flow”, Reviews in Chemical Engineering 21, (3-4) (2005) 133-164.
[18] Y. Y. Hsu, “On the size range of active nucleation cavities on a heated surface”, Journal of Heat Transfer 84 (1962) 207-216.
[19] G.P. Celata, M. Cumo, A. Mariani, “Experimental evaluation of the onset of subcooled flow boiling at high liquid velocity and subcooling”, International Journal of Heat and Mass Transfer (1997) 2879-2885.
[20] S. K. Saha, G.P. Celata, S. G. Kandlikar, “Thermofluid Dynamics of Boiling in Microchannels”, Advances in Heat Transfer 43 (2011) 77-226.
[21] E.J. Davis, G.H. Anderson, “The incipience of nucleate boiling in forced convection flow”, AICHE Journal 12 (4) (1966) 774-780.
[22] T. Sato, H. Matsumura, “On the condition on incipient subcooled boiling with forced convection”, Bulletin of JSME 7 (26) (1964) 392-398.
[23] A.E. Bergles, W.M. Rohsenow, “The determination forced convection surface boiling heat transfer“, Journal of Heat Transfer 86 (1964) 365-372.
[24] S.G. Kandlikar, S. Garimella, D. Li, S. Colin, M.R. King, “Heat Transfer and Fluid Flow in Minichannels and Microchannels”, Ed. Butterworth-Heinemann (Elsevier), Waltham, MA (USA) (2006) 221-228.
[25] D. Liu, P.S. Lee, S.V. Garimella, “Prediction of the onset of nucleate boiling in microchannel flow”, International Journal of Heat and Mass Transfer 48 (2005) 5134-5149.
[26] S.M. Ghiaasiaan, R.C. Chedester, “Boiling incipience in microchannels”, International Journal of Heat and Mass Transfer 45 (2002) 4599-4606.
[27] W.J. Marsh, I. Mudawar, “Predicting the onset of nucleate boiling in wavy free-falling turbulent liquid films”, International Journal of Heat and Mass Transfer 32 (2) (1989) 361-378.
[28] S.G. Kandlikar, “Nucleation characteristics and stability considerations during flow boiling in microchannels”, Experimental Thermal and Fluid Science 30 (5) (2006) 441-447.
[29] V. Gnielinski, “New equations for heat and mass transfer in turbulent pipe and channel flow” International Chemical Engineering. 16(2) (1976) 359-368.
[30] C.J. Geankoplis, “Transport Processes and Unit Operations”, Prentice Hall International, New Jersey (1993).
[31] S.W. Churchill, “Friction-factor equation spans all fluid-flow regimes”, Chemical Engineering 84 (1977) 91-92.
[32] I.L. Pioro, W. Rohsenow, S.S. Doerffer, “Nucleate pool-boiling heat transfer. I: review of parametric effects of boiling surface”, International Journal of Heat and Mass Transfer 47 (2004) 5033-5044.
[33] B. Verlaat, L. Zwalinski, R. Dumps, M. Ostrega, P. Petagna, T. Szwarc, “TRACI, a multipurpose CO_2 cooling system for R&D”, 10th IIF/IIR Gustav Lorentzen on Natural Working Fluids, Delft - The Netherlands, June 25-27 (2012).
[34] S.L. Qi, P. Zhang, R.Z. Wang, L.X. Xu, “Flow boiling of liquid nitrogen in micro-tubes: Part I – The onset of nucleate boiling, two-phase flow instability and two-phase flow pressure drop”, International Journal of Heat and Mass Transfer 50 (2007) 4999-5016.